American Journal of Environmental Science and Engineering
2026, Vol. 10, No. 4, pp. 150–163
https://doi.org/10.11648/j.ajese.20261004.15

Research Article

Magneto-responsive Poly (Ionic Liquid) Fe_3O_4@CS@P[VEIm]Br Nanoparticles for High-Efficiency Separation of Oil-Water Emulsions

Mingxin Zheng, Lei Wu, Liwen Gao, Ruxue Wu, Yueting Shuai, Ning Zhang*, Ping Cui

School of Chemistry and Chemical Engineering, Anhui University of Technology, Ma'anshan, China

Abstract

Discharging untreated emulsified oily wastewater directly into the environment may present potential hazards to both ecological stability and human health. Therefore, the development of efficient and recyclable demulsification materials for the treatment of emulsified oily wastewater is of considerable importance. In this study, Fe_3O_4 particles were selected as the substrate, and chitosan (CS) was grafted onto their surface via a cross-linking method. Poly (ionic liquids) were then stably anchored onto the chitosan-modified Fe_3O_4 through the synergistic effects of hydrogen bonding and electrostatic interactions. As a result, a magnetic-responsive poly (ionic liquid) composite particle, denoted as Fe_3O_4@CS@P[VEIm]Br, was successfully fabricated. The demulsification performance of the prepared composite particles was systematically evaluated. The experimental results showed that, under the conditions of an oil–water ratio of 10:90 and a salinity of 50 g/L, Fe_3O_4@CS@P[VEIm]Br at a dosage of 40 g/L achieved a demulsification efficiency of 99.0% within 10 min. In addition, after 10 consecutive reuse cycles, the demulsification efficiency remained above 93.0%, demonstrating excellent demulsification performance, salt tolerance, and recycling stability. Combined with the characterization results obtained from optical microscopy, contact angle measurements, and FT-IR analysis, a possible demulsification mechanism was proposed. The amphiphilic demulsifier can rapidly migrate to and accumulate at the oil-water interface, where it undergoes anion exchange with dodecylbenzene sulfonate in the surfactant. This process disrupts the original oil-water interfacial balance, promotes the rupture and coalescence of emulsion droplets, and thereby enables efficient emulsion separation. The results of this study indicate that Fe_3O_4@CS@P[VEIm]Br has promising application potential for the efficient treatment of emulsified oily wastewater, and the proposed mechanism provides useful insight into the design of magnetic-responsive poly (ionic liquid) demulsifiers with high efficiency, salt tolerance, and good reusability.

Keywords

Magnetic Poly Ionic Liquids, Ion Exchange, Amphiphilicity, Oil-water Emulsion Separation

*Correspondence: Ning Zhang (zhningy@163.com)

Received: 8 October 2026; **Accepted:** 27 October 2026; **Published:** 10 November 2026

Copyright: © The Author(s), 2026. Published by Science Publishing Group. This is an **Open Access** article, distributed under the terms of the Creative Commons Attribution 4.0 License (http://creativecommons.org/licenses/by/4.0/), which permits unrestricted use, distribution and reproduction in any medium, provided the original work is properly cited.

1. Introduction

Emulsified oily wastewater is widely generated in the petrochemical, metallurgical, machinery, and food industries [1-3]. Because it often contains surfactants to emulsify oil substances, it has the characteristics of difficult degradation, great harm and high environmental risk [4-8]. It is the most difficult type of treatment in oily residual liquid, and it is also one of the key and difficult points in industrial pollution prevention and control. How to effectively treat emulsified oil wastewater to achieve water resources protection and oil reuse is a worldwide scientific problem [9-12].

At present, the commonly used treatment methods of emulsified oil wastewater mainly include physical [13], chemical [14], and biological demulsification methods [15]. Physical methods such as microwave demulsification [16], membrane separation [17, 18] and ultrasonic separation [19] are pollution-free and versatile, but there are problems such as high cost and unsatisfactory results. The biological method uses biological metabolites with low energy consumption and high efficiency, but generally requires a long domestication cycle [20]; the chemical method mainly reduces the interfacial tension of the emulsion droplets by adding chemical demulsifiers, destabilizes the interfacial film, and facilitates droplet coalescence [21]. It offers notable advantages, including high efficiency and rapid operation. [22, 23]. However, chemical demulsifiers are mostly toxic and easy to cause secondary pollution in water bodies [24]. Therefore, in recent years, the preparation of high-efficiency, low-cost and easily recyclable chemical demulsifiers has become a research hotspot.

Ionic liquids (ILs) have the characteristics of strong solubility, good thermal stability and high chemical stability [25]. In particular, the precisely controllable hydrophilicity/hydrophobicity, polarity and surface activity make it a promising chemical demulsifiers [26]. Li [27] et al. evaluated nine halogenated ILs for oil-in-water (O/W) emulsion demulsification, and the demulsification efficiency exceeded 90% by 20 min. Sadighian [28] et al. synthesized a series of imidazolium-based ionic liquids, among which the Br-containing ionic liquids exhibited the highest demulsification efficiency, reaching 92%. Research shows that ionic liquids have a good demulsification effect, but there are also problems such as easy loss, unsatisfactory recycling effect and easy to cause secondary pollution of water. Based on this, some scholars have carried out research on the use of poly (ionic liquids) (PILs) for treating emulsified oily wastewater. For example, Ayman [29] et al. synthesized pyridine cationic PILs PEIDP by free radical polymerization, and the separation efficiency of O/W emulsion was almost 100%. However, PEIDP requires a demulsification time of up to 6 h and needs to be further recovered by membrane separation or sedimentation processes. Therefore, some scholars have combined ILs with magnetic particles to achieve convenient and fast magnetic recovery. Sadighian [30] et al. successfully prepared a new, environmentally friendly and easy-to-reuse Fe_3O_4@β-CD magnetic nanocomposite particles based on imidazole modification by chemical bond grafting method, and applied it to demulsifying and separating of crude oil water-in-oil (W/O) emulsions; it was found that 5000 ppm Fe_3O_4@β-CD@[ImSi-C10][Br] could achieve 92% demulsification efficiency for (30:70 vol%) W/O emulsion within 24 h. Chemical bond grafting is mainly connected by covalent bonds or coordination bonds, but its synthesis path is complex, requires multi-step reactions, has high cost, and may involve toxic reagents or strict conditions. In contrast, physical coating mainly achieves the combination of PILs and magnetic particles through physical adsorption, electrostatic interaction or van der Waals force. Liu [31] et al. used electrostatic interaction to coat ILs on cyclodextrin-functionalized magnetic dendritic polymer composites (MNP@PAMAM@CD@IL). This material exhibits high adsorption capacity and can also be rapidly recovered through its magnetic responsiveness. Cheng [32] et al. PILs were physically coated on molecular sieves and applied in a T-type device with hydrophilic and hydrophobic membranes for demulsifying and separating water-in-oil emulsions, achieving a demulsification efficiency of up to 99% within 3 h. It can be seen that the physical coating method constitutes a facile and efficient route for synthesizing magnetically responsive PILs. However, there are still few reports on the direct separation of emulsified oil wastewater. Therefore, achieving stable and uniform physical coating of PILs onto magnetic particles, along with efficient separation of emulsified oil wastewater, remains an urgent challenge.

Therefore, in this study, a novel and straightforward approach was adopted to successfully prepare the magnetic responsive PILs Fe_3O_4@CS@P[VEIm]Br. The influence of demulsifiers dosage, demulsification time, alkyl chain length and emulsion concentration on demulsification performance were investigated. Additionally, the salt tolerance and recyclability of the magnetic response demulsifier were investigated. Finally, the demulsification mechanism of the demulsifier was revealed by contact angle, infrared spectroscopy and optical microscopy analysis, which provided theoretical guidance for designing highefficiency demulsifiers.

2. Experimental

2.1. Materials

Iron trichloride, hexahydrate ($FeCl_3$ $6H_2O$, purity ≥ 99.0%), ethylene glycol (EG, purity ≥ 98.0%), glacial acetic acid (HAc, purity ≥ 99.5%), glutaraldehyde (GA, purity ≥ 50.0%), azobisisobutyronitrile (AIBN, purity ≥ 98.0%), 1-vinyl-3-ethylimidazolium bromide ([VEIm]Br, purity ≥ 99.0%) were supplied by Shanghai Macklin Biochemical Technology Co., Ltd. Ethanol (EtOH, purity ≥ 99.7%), anhydrous sodium acetate (CH_3COONa, purity ≥ 99.0%), chitosan (CS, deacetylation

degree ≥ 95.0%), toluene (purity ≥ 99.5%) were acquired from Sinopharm Group Chemical Reagents Co., Ltd. Polyethylene glycol (PEG, Mn = 4000) and 1-vinyl-3-butylimidazolium bromide ([VBIm]Br, purity ≥ 98.0%) were supplied by Shanghai Aladdin Biochemical Technology Co., Ltd. 1-Vinyl-3-octylimidazolium bromide ([VOIm]Br, purity ≥ 98.0%) was supplied by Zhengzhou Aikem Chemical Co., Ltd. All experiments were conducted using deionized water, and all chemical reagents were not purified.

2.2. Synthesis of Demulsifiers

3.6g CH_3COONa, 1.35 g $FeCl_3$ $6H_2O$, 1.0 g polyethylene glycol-4000 and 40 mL ethylene glycol were introduced into a 100 ml beaker, respectively. The uniform mixed solution was formed by ultrasonic oscillation for 30 min, then transferred to a 100 mL hydrothermal reactor and positioned a vacuum drying oven. The reaction was conducted at 200 ℃ for 8 h, after which the system was allowed to cool to 25 ℃. The product was rinsed alternately with ethanol and water 3 times and finally vacuum-dried at 60 ℃ for 24 h to yield Fe_3O_4.

Fe_3O_4 was dispersed in 20 mL of 1% acetic acid, and then 20 mg of chitosan was added. Following ultrasonic homogenization, the suspension was transferred into a three-necked flask, where crosslinking was initiated by adding 2 mL of 25% glutaraldehyde solution and maintained at 25 ℃ for 4 h. The resulting product was alternately washed with deionized water and ethanol three times to yield Fe_3O_4@CS.

The ionic liquid [VEIm]Br 0.35 g, AIBN 0.02 g, a 50 mL three-necked round-bottom flask was charged with 25 mL of deionized water, and the contents were stirred at 25 ℃ for 30 min to achieve homogeneous mixing. Subsequently, 0.2 g of Fe_3O_4@CS was introduced, and the reaction was allowed to proceed under stirring at 80 ℃ for 12 h. Upon completion, the product was alternately washed three times with deionized water and acetone. The final polymerized product, designated Fe_3O_4@CS@P[VEIm]Br, after vacuum drying at 65 ℃ for 12 h, the product was obtained. The synthetic pathway is shown in Figure 1.

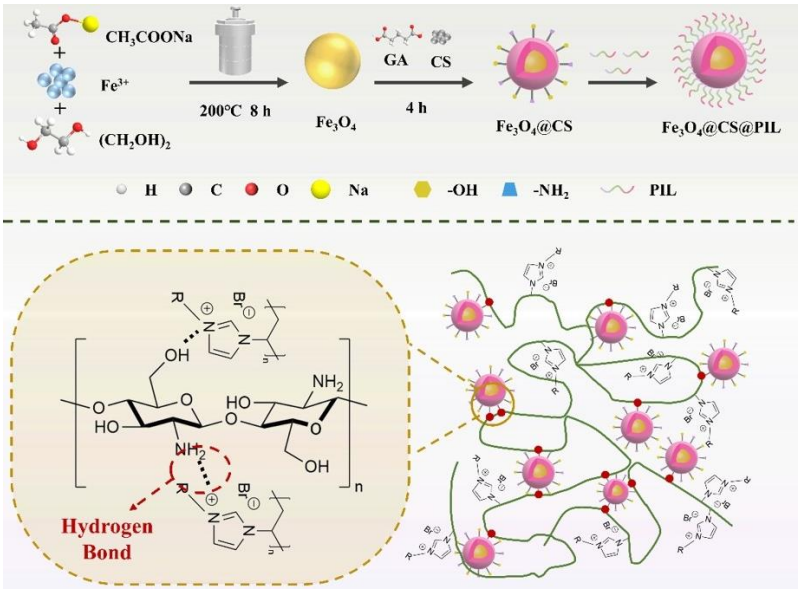


Figure 1. *Preparation procedure forFe_3O_4@CS@P[VEIm]Br demulsifier particles.*

2.3. Preparation of the O/W Emulsions

SDBS was introduced into a toluene–water mixture at a mass fraction of 0.01 wt.%, and the resulting mixture was ultrasonicated for 30 min to form O/W toluene emulsions with concentrations of 0.1, 0.2, 0.4, 0.6 and 0.8 mL/L, respectively. As illustrated in Figure 2(a), UV-visible spectroscopy revealed a characteristic absorption peak for toluene at 261 nm. A calibration curve was constructed from the characteristic peak intensities measured at different toluene concentrations, as illustrated in Figure 2(b). Eq. (1) was subsequently obtained through curve fitting.

$$A = 0.925C - 0.0045 \quad (1)$$

In the formula, A and C represent the absorbance at 261 nm and the corresponding toluene concentration, respectively. The resulting calibration curve yielded an R^2 value of 0.9996.

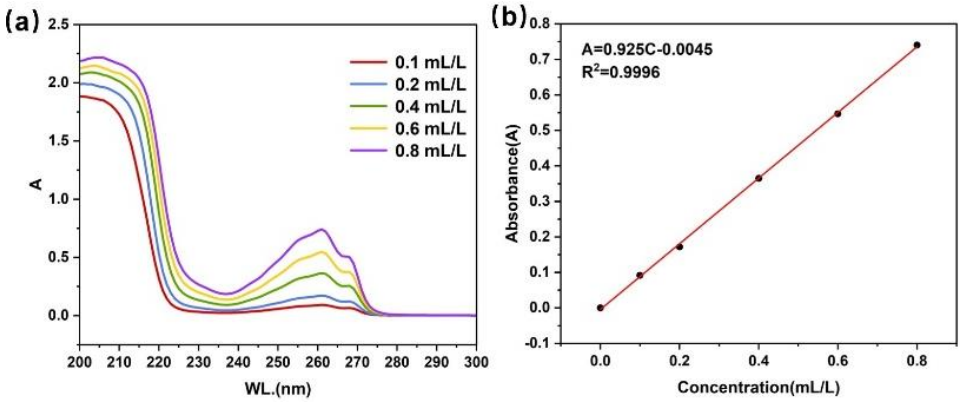


Figure 2. *(a) UV absorption profiles of toluene emulsions with varying concentrations. (b) Calibration curve of toluene emulsion.*

2.4. Demulsification Test

In the process of studying the demulsification performance of emulsified oil wastewater, a 5 mL aliquot of the emulsion to be separated was transferred into a glass bottle, and the magnetic response PILs demulsifiers was added to it. After shaking for a certain time, the mixture was subjected to magnetic separation, and the clear liquid was taken for ultraviolet spectrum analysis. Therefore, using the standard curve, the toluene concentration was determined from the absorbance of the target emulsion measured before and after separation. The specific demulsification efficiency is given by Eq. (1).

$$\text{Demulsification efficiency (\%)} = \frac{C_0 - C}{C_0} \quad (2)$$

where C_0 is the original oil concentration (mL/L) of the before-treatment emulsion and C is the oil concentration (mL/L) of the after-treatment emulsion.

2.5. Characterization

Size and morphology of different magnetic particles were characterized by scanning electron microscopy (SEM, Regulus-8100, Hitachi) and transmission electron microscopy (TEM, HT-7800, Hitachi), and the particle size distribution of each stage was measured by Image J software. The spatial distribution of elements was observed by EDS (AXIS ULTRA DLD). The roughness features and microscopy of the magnetic particles was detected by atomic force microscopy (AFM, cypher). The chemical groups of the different magnetic particles were examined by fourier transform infrared spectrometer (FT-IR, IS50) with the KBr pellet method. The thermal stability of different magnetic particles was tested by thermogravimetric (TG) analyzer (Thermax 700). The hysteresis loop of different magnetic particles was determined by using a vibrating sample magnetometer (VSM, LakeShore7404, USA) at 25 ℃. The zeta potential of the different magnetic particles was determined by Malvern Nanosizer instrument at various pH levels (Zetasizer Nano ZS90, Malvern Instruments Company, UK). Contact angle measurements for the different magnetic particles were performed with an XG-CAME instrument, and the average value was recorded three times. The optical microscope (MS1000T, Nikon) was employed to examine the emulsion at different stages during the demulsification process.

3. Results

3.1. Micromorphology and Composition

The microstructures of Fe_3O_4, Fe_3O_4@CS and Fe_3O_4@CS@P[VEIm]Br particles are shown in Figure 3. As illustrated in Figure 3(a), the hydrothermally synthesized Fe_3O_4 particles are spherical with a homogeneous particle size. The rough structure of the Fe_3O_4 surface can be observed from the Figure 3(a') TEM image, which is also conducive to further grafting with CS. As observed in Figure 3 (b and b'), the Fe_3O_4@CS magnetic particles have a larger particle size than bare Fe_3O_4, confirming the successful surface attachment of chitosan onto Fe_3O_4. Figure 3 (c and c') show the micro-morphology of the Fe_3O_4@CS@P[VEIm]Br. From Figure 3(c'), the more obvious light and dark structure of the sphere's exterior can be observed clearly, indicating that P[VEIm]Br was successfully coated onto Fe_3O_4@CS. As presented in Figure 3(h), the particle size distributions of Fe_3O_4, Fe_3O_4@CS and Fe_3O_4@CS@P[VEIm]Br were calculated using Image J software to be falling within 70 ~ 80 nm, 100 ~ 110 nm and 110 ~ 120 nm, respectively, and the average diameters of the three magnetic particles were 72.6 nm, 102.8 nm and 112.4 nm, respectively, showing a gradual increase trend. This is due to the fact that the surface of Fe_3O_4@CS@P[VEIm]Br was coated with CS and P[VEIm]Br in turn. The EDS test results show that Fe_3O_4@CS@P[VEIm]Br contains three elements of Fe, O and C, and is evenly distributed on the particles. In addition, the existence of the characteristic element Br in PILs was also shown in the spectrum, which further indicated the successful attachment of PILs onto the surface of Fe_3O_4@CS.

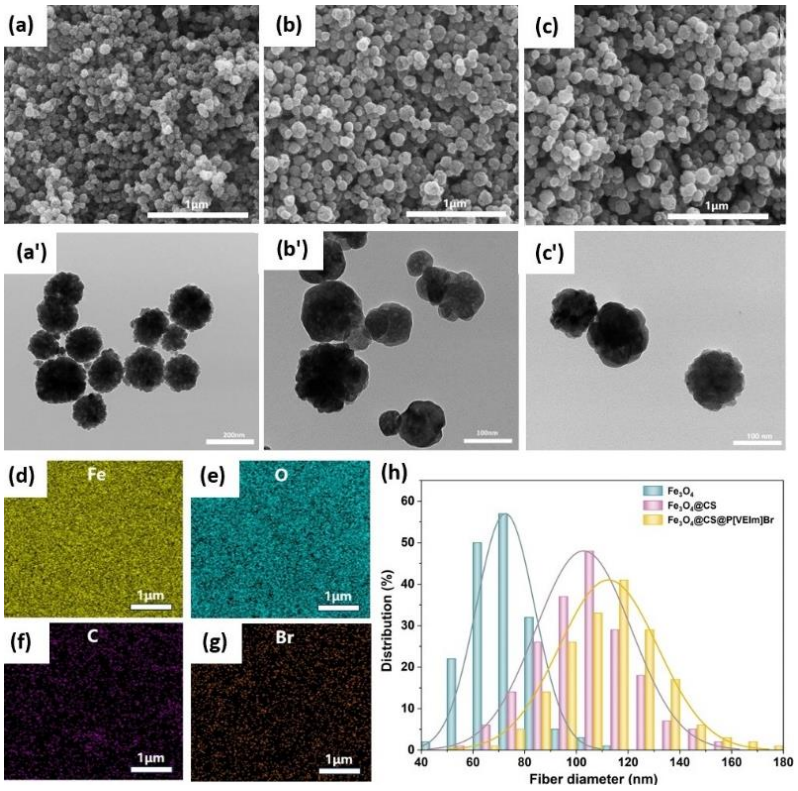


Figure 3. *The TEM and SEM images of three demulsifier particles (a, a') Fe_3O_4. (b, b') Fe_3O_4@CS, (c, c') Fe_3O_4@CS@P[VEIm]Br were obtained. (d-g) EDS scanning image of Fe_3O_4@CS@P[VEIm]Br. (h) Particle size distribution of Fe_3O_4, Fe_3O_4@CS, Fe_3O_4@CS@P[VEIm]Br.*

The surface roughness of Fe_3O_4, Fe_3O_4@CS and Fe_3O_4@CS@P[VEIm]Br magnetic particles was tested by atomic force microscopy. As illustrated in Figure 4(a, a'), the Fe_3O_4 surface is relatively flat, with a roughness value of 9.210 nm as determined by Gwyddion software. In Figure 4 (b, b'), numerous uniformly distributed "peak" structures appeared on Fe_3O_4@CS, and the roughness value was measured to be 1.638 nm. As depicted in Figure 4 (c, c'), the surface of Fe_3O_4@CS@P[VEIm]Br exhibits numerous fine and distinct protrusions. Compared with Fe_3O_4@CS, the surface microstructure of Fe_3O_4@CS@P[VEIm]Br changed significantly, exhibiting a roughness of 0.879 nm. The above results show that with the increase of CS and P[VEIm]Br coating layers, the microstructure and roughness of magnetic PILs have changed accordingly.

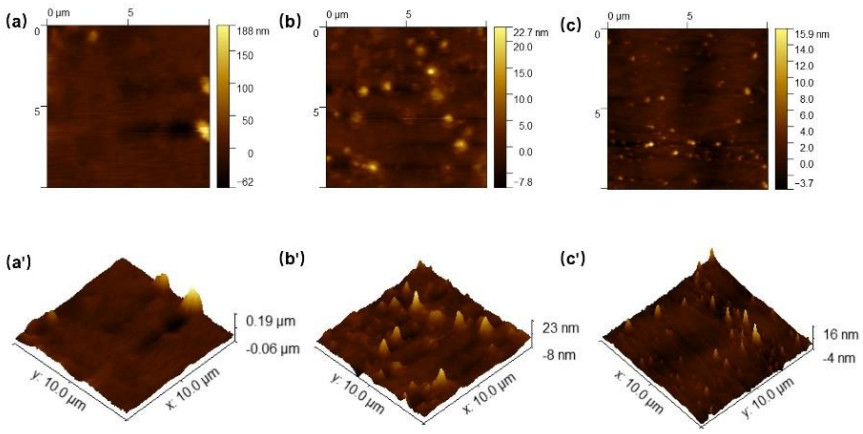


Figure 4. *(a, a') Fe_3O_4, (b, b') Fe_3O_4@CS, (c, c') Fe_3O_4@CS@P[VEIm]Br AFM images.*

3.2. FT-IR

In order to analyze and identify the functional group structure of Fe_3O_4, Fe_3O_4@CS and Fe_3O_4@CS@P[VEIm]Br magnetic particles, the infrared spectrum test was carried out and the spectral curve was drawn. As illustrated in Figure 5(a), the absorption peak at 575 cm^{-1} is characteristic of the Fe-O stretching vibration [29], which confirms the successful preparation of the Fe_3O_4 substrate. At the same time, in the infrared spectrum of Fe_3O_4@CS, two additional peaks are detected near 1076 cm^{-1} and 883 cm^{-1}, which were mainly ascribed to the C−O stretching vibration of chitosan and the skeleton vibration of the glycosidic bond [34]. This result proved that CS was successfully coated onto magnetic particles. In the spectral curve of Fe_3O_4@CS@P[VEIm]Br, the characteristic vibration peaks of C−H bond and C=N bond appeared at 2861 cm^{-1} and 1638 cm^{-1} [30, 35], respectively, confirming that PILs were successfully anchored onto the surface of Fe_3O_4@CS particles. The spectrum reveals the −OH stretching band at 3445 cm^{-1} shifts to the right to 3430 cm^{-1}, and the stretching vibration peak of the C=N bond shifts from 1639 cm^{-1} to 1631 cm^{-1}. This phenomenon is mainly ascribed to hydrogen bonding between PILs and the abundant $-NH_2$ and −OH groups on the CS surface [36].

3.3. Magnetic Property

For magnetic demulsifiers, the magnetic properties are an important factor influencing their demulsification and recovery. Therefore, the magnetic characteristics of Fe_3O_4, Fe_3O_4@CS, and Fe_3O_4@CS@P[VEIm]Br were analyzed. The results are presented in Figure 5(b). The hysteresis loop passes through the origin, indicating that the demulsifiers do not have residual magnetization and coercivity, and thus exhibit superparamagnetic characteristics [30]. The saturation magnetization values of Fe_3O_4, Fe_3O_4@CS, and Fe_3O_4@CS@P[VEIm]Br are 72.8, 67.5 and 65.0 emu/g respectively, showing a decreasing trend. This is mainly due to the further grafting of non-magnetic CS and PILs. Fe_3O_4@CS@P[VEIm]Br exhibits magnetic response characteristics, enabling its separation of the emulsion to be conveniently recovered through an external magnetic field.

3.4. Thermal Stability

Figure 5(c) TGA diagram shows the thermal stability of Fe_3O_4, Fe_3O_4@CS and Fe_3O_4@CS@P[VEIm]Br magnetically responsive demulsifiers particles. In the initial stage of pyrolysis, the three demulsifiers particles showed a mass loss of 1.3% ~ 2.4% in the temperature range of 30 ~ 150℃, which was likely due to the desorption of physically adsorbed water on the particle surface and the volatilization of residual solvents. In the second stage, Fe_3O_4@CS and Fe_3O_4@CS@P[VEIm]Br particles exhibit different thermal decomposition behaviors in the high temperature region. Firstly, the secondary weight loss (about 6%) of Fe_3O_4@CS within 220 ~ 600 ℃ is assigned to the thermal decomposition of the CS coating layer. The breakage of the main chain of the glycosidic bond and the decomposition of the side chain group together lead to a decrease in mass, which confirms the successful coating of CS. In addition, the weight loss rate of Fe_3O_4@CS@P[VEIm]Br at 220 ~ 570 ℃ is about 8%, which is mainly due to the combined effect of imidazolium side chain breakage and main chain decomposition in the outermost coating layer PIL, which further confirms that the P[VEIm]Br is successfully coated on the surface of Fe_3O_4@CS.

3.5. Zeta Potential

To investigate the electrostatic interaction between magnetic nanoparticles and PIL as well as its influence on surface charge, Zeta potential tests were carried out on three demulsifiers: The Zeta potential experimental results for Fe_3O_4, Fe_3O_4@CS and Fe_3O_4@CS@P[VEIm]Br are presented in Figure 5(d). Fe_3O_4 exhibits a zeta potential of −16.8 mV, which is mainly attributable to surface hydroxyl groups on Fe_3O_4 prepared by hydrothermal method. Upon CS coating, the zeta potential of Fe_3O_4@CS shifted to −15.9 mV. This decrease is attributed to the protonation of amino group ($-NH_2$) on the CS molecular chain will be protonated ($-NH_3^+$) under acidic conditions to make it positively charged, so the negative Zeta potential decreases. The electronegativity was further reduced to −7.6 mV after grafting PILs. The main reason for this change was the electrostatic adsorption between cationic $P[VEIm]^+$ and negatively charged Fe_3O_4@CS, resulting in charge neutralization. Therefore, the above experimental results further proved the successful grafting of CS and coating of PILs.

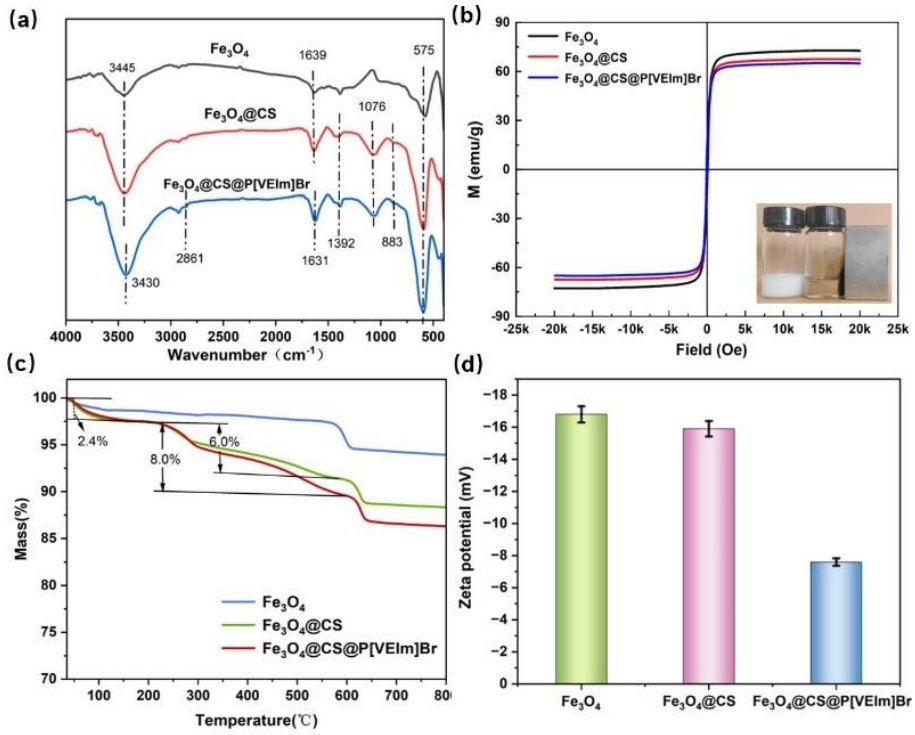


Figure 5. *Fe_3O_4、Fe_3O_4@CS 和 Fe_3O_4@CS@P[VEIm]Br demulsifier particles (a) FT-IR; (b) VSM (illustrated as image of original emulsion and emulsion after demulsification). (c) TGA analysis. (d) Zeta potential test.*

3.6. Demulsification Performance Test

To investigate the effect of varying alkyl chain lengths (C= 2, 4, 8) on the demulsification effect of magnetically responsive PILs, the demulsification efficiency of Fe_3O_4@CS@P[VEIm]Br, Fe_3O_4@CS@P[VBIm]Br and Fe_3O_4@CS@P[VOIm]Br on emulsified oil wastewater with a concentration of 10:90 at 10 min was tested respectively. The results are illustrated in Figure 6(a). When the dosage was 20 g/L, the demulsification efficiencies of Fe_3O_4@CS@P[VEIm]Br 、 Fe_3O_4@CS@P[VBIm]Br and Fe_3O_4@CS@P[VOIm]Br were 70.5%, 86.2% and 96.3%, respectively. At a dosage of 40 g/L, demulsification efficiencies of 95.3%, 98.1% and 98.3% were achieved. As illustrated in Figure 6(b), with increasing emulsion concentration, Fe_3O_4@CS@P[VEIm]Br showed the highest demulsification efficiency for 10:90 O/W emulsion. The stability test results of emulsified oil wastewater showed that prolonged stability was not achievable after increasing to 12:88. Based on this, the demulsification performance of 10:90 emulsified oil wastewater was further explored.

In this study, the effects of different dosage (10, 20, 30, 40, 50 and 60 g/L) and time (5, 10, 30, 60 and 120 min) of Fe_3O_4@CS@P[VEIm]Br on demulsification were investigated. It is evident from Figure 6(c) that when the dosage is 10 g/L, the demulsification rate is 60.2% at 5 min, and the demulsification rate gradually increases with time. At a demulsification time of120 min, the demulsification rate was 72.6%. This is because as demulsification time increases, Fe_3O_4@CS@P[VEIm]Br can migrate more to the oil-water interface, and interact with the emulsified oil droplets to promote the destabilization of the emulsion, thereby improving the demulsification efficiency. At a demulsification time of 10 min, the demulsification rate gradually increased with increasing dosage. Among them, at a dosage of 10 g/L, the demulsification rate was 62.6%; at 40 g/L, the rate was 98.1%. Subsequently, with further increases in dosage and demulsification time, the demulsification rate remained basically unchanged. Figure 6(d) shows the demulsification efficiency of Fe_3O_4, Fe_3O_4@CS and Fe_3O_4@CS@P[VEIm]Br at the dosage of 40 g/L and demulsification time of 10 min, which are 54.8%, 50.3% and 98.1%, respectively. The comparison results show that PILs have obvious demulsification effect.

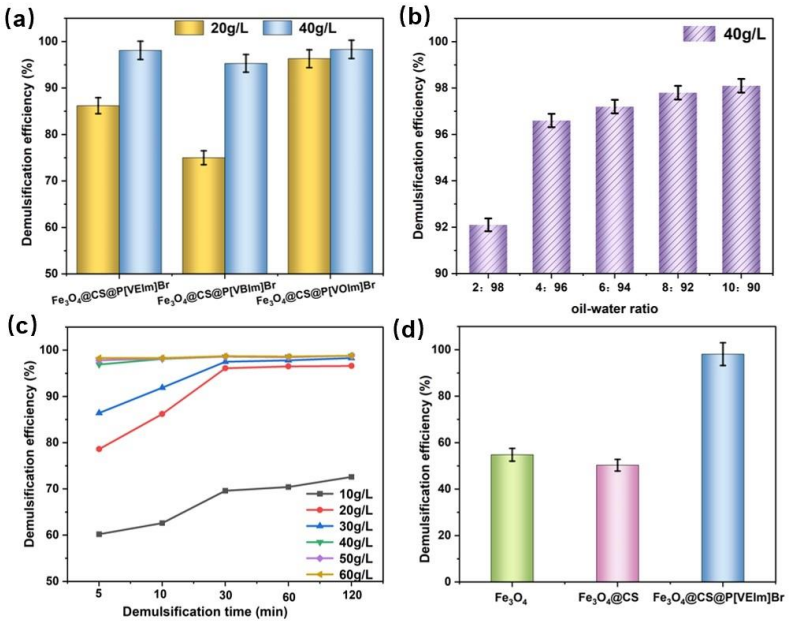


Figure 6. *(a) The demulsification efficiency of Fe_3O_4@CS@P[VEIm]Br、Fe_3O_4@CS@P[VBIm]Br and Fe_3O_4@CS@P[VOIm]Br at 10 min. (b) The demulsification efficiency of Fe_3O_4@CS@P[VEIm]Br for O/W emulsions at different concentrations. (c) The demulsification efficiency of Fe_3O_4@CS@P[VEIm]Br with different dosage and demulsification time. (d) Demulsification efficiency of Fe_3O_4、Fe_3O_4@CS and Fe_3O_4@CS@P[VEIm]Br.*

To investigate the effect of salinity on demulsification, NaCl solutions of 1, 2, 3, 4, 5, 10 and 50 g/L were added to the target emulsified oil wastewater. Figure 7(a) is the demulsification efficiency of Fe_3O_4@CS@P[VEIm]Br demulsifiers at different salinities. Under the demulsification condition of 10 min, when the salinity is 1 g/L, the demulsification rate is 60.2%; when the salinity is 50 g/L, the demulsification rate is 99.0%. As salinity increased, the demulsification rate gradually increases. This phenomenon arises because, under high-salinity conditions, salt anions in the aqueous phase diminish the electrostatic repulsion among imidazolium ring cations, thereby enhancing the adsorption of PILs at the oil–water interface and leading to efficient demulsification**.** As shown in Figure 7(b), in order to explore the recycling performance of Fe_3O_4@CS@P[VEIm]Br demulsifiers, Fe_3O_4@CS@P[VEIm]Br was magnetically separated and recovered after each use, and then soaked in NaBr solution (1000 mg L^{-1}), regenerated by ion exchange with Br^- in NaBr solution, and its recycling performance was tested. The results indicate that the demulsification efficiency decreases gradually as the cycle number increases. After 10 cycles of demulsification, the demulsification rate of Fe_3O_4@CS@P[VEIm]Br remained above 93.2%, showing good reusability.

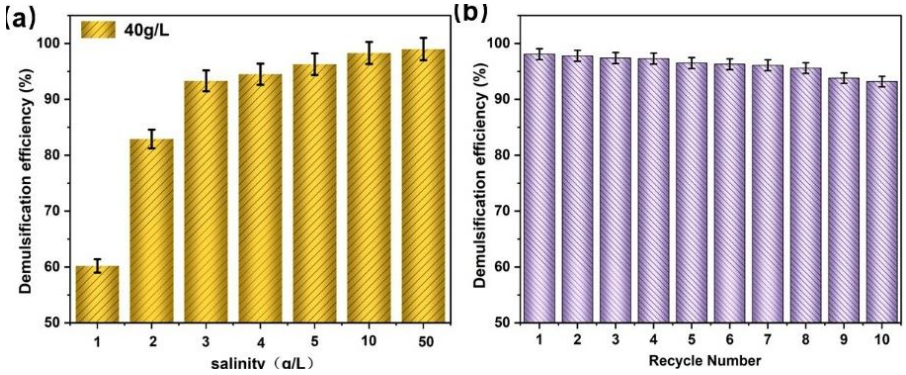


Figure 7. *The demulsification efficiency of Fe_3O_4@CS@P[VEIm]Br demulsifier particles (a) at different salinities. (b) Recycling performance.*

In Table 1, the Fe_3O_4@CS@P[VEIm]Br magnetically responsive PILs demulsifiers prepared in this study was compared with the emulsion oil wastewater separation materials reported in the literature. The comparison results show that the demulsifiers has excellent performance in separation speed, demulsification efficiency and recycling performance, showing good research value and application potential.

Table 1. *The comparison of demulsification efficiency between this work and other literatures.*

Demulsifiers	Demulsifying Mechanism	Oil: Water	Time	Demulsification Efficiency	Reuse Performance (frequency)	Ref.
Fe_3O_4@CPAM	Coupling and Synergy	7:3	30 min	99.10%		[37]
Fe_3O_4@CS@NaOL	Electrostatic Adsorption	1:99		91%	80% (8)	[34]
$CuFe_2O_4$/MWCNT	π-π Bond Bonding	viscous oil	30 min	95%	90% (7)	[38]
MPCs@PVA	Adsorption-bridging	1:200	1 h	95.13%	80% (6)	[39]
P[IL]@MCs	Adsorption Displacement	3:7	2 h	99.5%	89% (5)	[33]
Fe_3O_4@PDA-EDEP	Ion Exchange	5:95	80 min	99.55%	99% (8)	[40]
PPBD and PPBH(IL)	Adsorption Displacement	3:7	2 h	96.34%		[41]
DEBIL	Electrostatic Attraction	3:7	2 h	98.5%		[42]
Y6/Y12/Y18	Electrostatic Attraction		90 min	100%		[43]
PE-CL(Gemini)	Adsorption Displacement	1:1	3 h	100%		[44]
Fe_3O_4@β-CD@[Im-Cn][Br]	Adsorption Displacement	3:7	24 h	92%	82% (5)	[25]
Fe_3O_4@CS@P[VEIm]Br	Electrostatic Attraction	10:90	10 min	98.1%	93.2% (10)	This work

3.7. The demulsification Mechanism

To explore the wettability of the demulsifiers particles, the water contact angle (WCA) and oil contact angle (OCA) of Fe_3O_4, Fe_3O_4@CS and Fe_3O_4@CS@P[VEIm]Br were measured using a contact angle goniometer, with the results presented in Figure 8(a). The test method is to add water or oil droplets to the surface of the compacted demulsifiers particles and record the static contact angle changes. The WCA test value of Fe_3O_4 is 53.5 °. After coating with CS and PILs in turn, the WCA of Fe_3O_4@CS and Fe_3O_4@CS@P[VEIm]Br decreased to 30.9 ° and 17.9 °, respectively. The significant reduction of WCA is mainly attributed to the introduction of amino groups in CS and hydrophilic Br^- in PILs, which greatly enhances the surface hydrophilicity of the composite material. This gradual improvement in hydrophilicity is conducive to the dispersion of demulsifiers particles in the aqueous phase. In order to evaluate the lipophilicity, soybean oil was dropped onto the surface of Fe_3O_4, Fe_3O_4@CS and Fe_3O_4@CS@P[VEIm]Br demulsifiers particles, and the test values of OCA were 86.3 °, 100.0 ° and 42.0 °, respectively. The decrease of OCA test value of Fe_3O_4@CS@P[VEIm]Br demulsifiers particles is mainly due to the fact that the ethyl and vinyl groups in P[VEIm]Br are non-polar alkyl chains, which makes Fe_3O_4@CS@P[VEIm]Br show good lipophilicity. In summary, Fe_3O_4@CS@P[VEIm]Br exhibits excellent amphiphilicity, which is beneficial to adsorb at the O/W emulsion interface, reduce the interfacial tension, and achieve efficient demulsification.

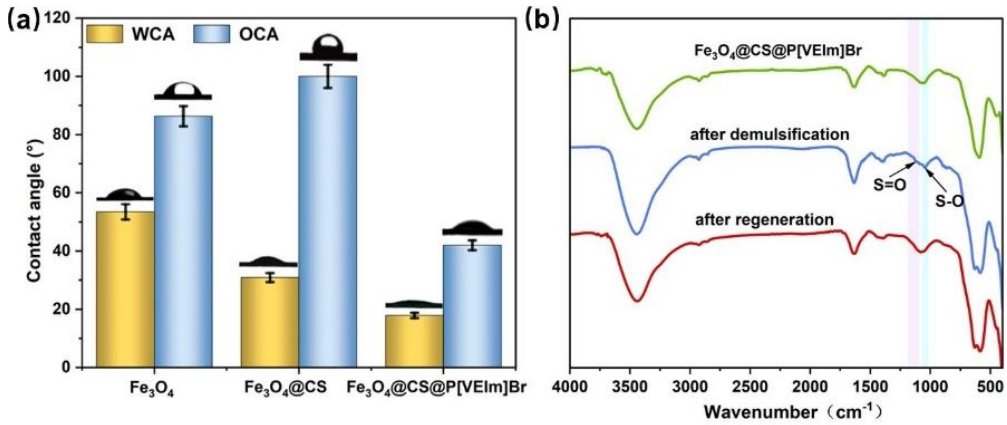


Figure 8. *(a) The water and oil contact angles of Fe_3O_4, Fe_3O_4@CS and Fe_3O_4@CS@P[VEIm]Br were tested. (b) FT-IR test of Fe_3O_4@CS@P[VEIm]Br before demulsification, after demulsification and after regeneration.*

In order to further explore the demulsification mechanism, we carried out FT-IR characterization of Fe_3O_4@CS@P[VEIm]Br demulsifiers before and after use. Following demulsification, the magnetically responsive nanoparticles in Figure 8(b) display two new IR absorption features at 1055 cm^{-1} and 1126 cm^{-1}, which are caused by the tensile vibration of S=O and S-O in sodium dodecyl benzene sulfonate. According to the results, it can be inferred that the anion exchange occurred between the dodecylbenzene sulfonate ion (DS^-) in the emulsion and the Br^- in the magnetically responsive PILs. This exchange behavior destroys the stability of the original oil-water interface, thereby promoting the coalescence of emulsion droplets and achieving oil-water separation. Furthermore, the used demulsifiers can be regenerated by ion exchange with Br^- in NaBr solution. The FT-IR spectrum of the regenerated demulsifiers showed that the characteristic absorption peak of the original S=O bond disappeared, indicating that DS^- had desorbed from the surface of the material. The appearance and disappearance of the above characteristic peaks confirmed the ion exchange mechanism during demulsification, and the previous studies showed that the demulsifier exhibited good recycling performance.

To investigate the demulsification process of the demulsifiers, an optical microscope was used to observe the microscopic morphology of the emulsified oil droplets at different demulsification stages. As seen in Figure 9(a), the macroscopic state of the emulsified oil wastewater with an oil-water ratio of 10:90 is milky white, and it is presented as evenly distributed emulsion droplets under a microscope. After adding Fe_3O_4@CS@P[VEIm]Br and shaking for 10 min, as can be observed from Figure 9(b), the emulsified oil wastewater was brown, and the emulsion droplets showed obvious aggregation under the microscope. In enlarged Figure 9(c) and (d), it can be clearly observed that the magnetic demulsifiers is adsorbed at the interface of the emulsified oil. In further enlarged Figure 9(d'), droplet coalescence was observed. Under the action of oscillation, the amphiphilic demulsifiers ions can move toward the oil-water boundary more efficiently, and undergo anion exchange with the surfactant to break the original equilibrium state of the interface, inducing rupture, coalescence and continuous fusion of emulsion droplets into larger droplets. In Figure 9(e), the emulsified oil wastewater became clear after magnetic separation, and almost no emulsion droplets were observed under a microscope.

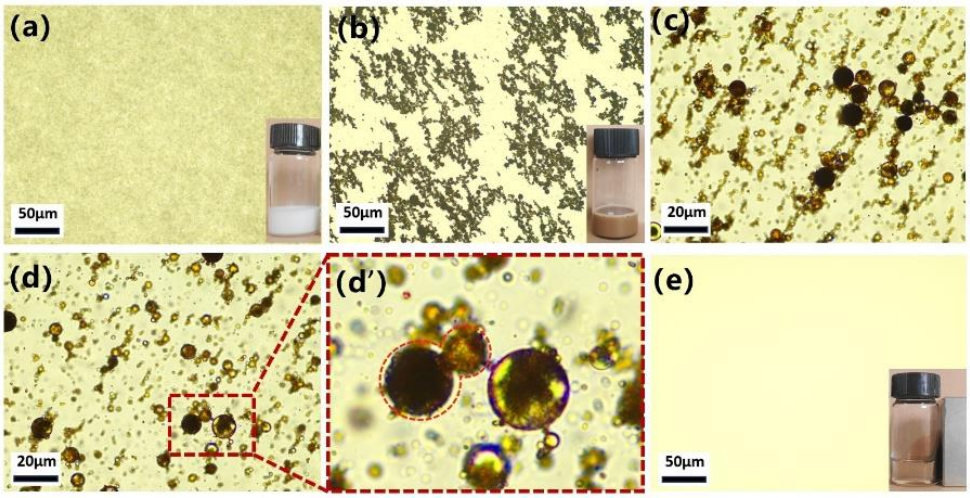


Figure 9. *The optical microscope of O/W emulsion at different demulsification stages (a) The microscope of the original emulsion. (b) Add 40 g/L Fe_3O_4@CS@P[VEIm]Br to the emulsion and shake the microscope after 5 min. (c, d) is the enlarged microscope image of Figure (b). (d') is the further enlarged graph of Figure (d). (e) Microscopic image of emulsion after magnetic separation.*

The separation performance and underlying mechanism of Fe_3O_4@CS@P[VEIm]Br toward emulsified oil are illustrated in Figure 10. During the formulation of the O/W emulsion, SDBS was introduced into the oil-water mixture as a representative anionic surfactant. With its unique amphiphilic structure, SDBS molecules will be quickly adsorbed at the oil–water interface, thereby stably dispersing the oil droplets in water. and finally form a stable emulsion. 40 g/L Fe_3O_4@CS@P[VEIm]Br demulsifiers was added to the above prepared emulsion and oscillated for 10 min. Because the amphiphilic demulsifiers has good dispersion in the oil-water emulsion and can quickly adsorb at the oil-water interface. The anion exchange occurred between Br^- in Fe_3O_4@CS@P[VEIm]Br demulsifiers and DS^- in surfactant, which destroyed the interfacial equilibrium of emulsion droplets and caused the interfacial film to break under the action of oscillation, resulting in oil droplet flocculation and coalescence. Finally, the Fe_3O_4@CS@P[VEIm]Br demulsifiers particles were conveniently recovered by an external magnetic field.

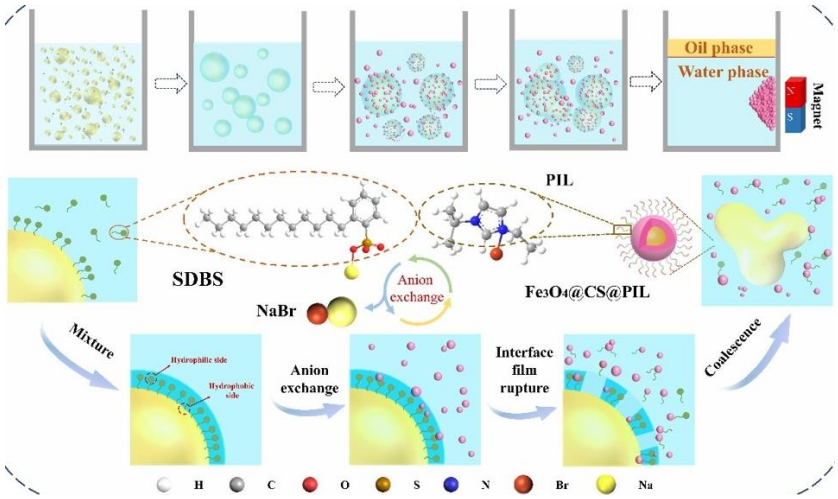


Figure 10. *Demulsification separation process and demulsification mechanism of Fe_3O_4@CS@P[VEIm]Br towards emulsified oil wastewater.*

4. Conclusion

In this study, Fe_3O_4@CS@P[VEIm]Br was successfully synthesized by grafting chitosan with rich amino and hydroxyl groups by cross-linking method, and further coating PILs on the surface of magnetic nanoparticles by hydrogen bonding and electrostatic synergy. A new type of magnetic responsive PILs Fe_3O_4@CS@P[VEIm]Br with simple synthesis route

and low cost was successfully synthesized. The bottle tests showed that Fe_3O_4@CS@P[VEIm]Br has good demulsification effect at high-concentration emulsion and salinity. In particular, when the dosage of Fe_3O_4@CS@P[VEIm]Br is 40 g/L, the optimal demulsification rate within 10 min can reach 99.0% when the O/W emulsion with the ratio of 10:90 and salinity of 50 g/L is treated. In addition, the demulsification efficiency of the demulsifiers is still above 93% after 10 cycles, showing good recycling performance. The results of contact angle test showed that Fe_3O_4@CS@P[VEIm]Br had good amphiphilicity. Combined with optical microscope and FT-IR test before and after demulsification, the demulsification mechanism can be concluded as follows: excellent amphiphilic Fe_3O_4@CS@P[VEIm]Br can be quickly adsorbed to the oil-water interface, so that Br^- in the demulsifiers can exchange with DS^- in SDBS to destroy the oil-water interface balance, thus achieving efficient demulsification. The high demulsification rate, salt tolerance and good reusability make Fe_3O_4@CS@P[VEIm]Br shows broad application potential for treating emulsified oily wastewater.

Abbreviations

ILs	Ionic Liquids
PILs	Poly Ionic Liquids
W/O	Water-in-oil
O/W	Oil-in-water
WCA	Water Contact Angle
OCA	Oil Contact Angle

Acknowledgments

The authors sincerely thank Associate Professor Ning Zhang for her valuable suggestions on the experimental design and manuscript preparation. We also sincerely thank all participants for their assistance with the demulsification tests and characterization measurements.

Author Contributions

Zhang Ning: Funding acquisition, Project administration, Resources, Supervision, Writing – review & editing

Cui Ping: Funding acquisition, Project administration, Supervision

Zheng Mingxin: Data curation, Investigation, Methodology

Wu Ruxue: Conceptualization, Data curation, Investigation, Methodology, Writing – original draft

Shuai Yueting: Formal Analysis, Methodology, Software

Gao Liwen: Funding acquisition, Project administration, Supervision, Validation

Wu Lei: Formal Analysis, Methodology

Funding

This work is supported by the National Natural Science Foundation of China (Project 52503125, 22478004) and the Undergraduate Innovation and Entrepreneurship Training Program of Anhui Province (No. 202310360038).

Data Availability Statement

The data is available from the corresponding author upon reasonable request.

Conflicts of Interest

The authors declare no conflicts of interest.

References

[1] Rozhkova Y, Lekomtsev A, Lisin V. Comprehensive review of demulsifiers based on magnetic nanoparticles for oil-water and water-oil separation. International Journal of Engineering, Transactions B: Applications, 2024, 37(5): 904-919. https://doi.org/10.5829/ije.2024.37.05b.09

[2] Zhang T, Li Z, L ü Y. Recent progress and future prospects of oil-absorbing materials. Chinese Journal of Chemical Engineering, 2019, 27(6): 1282-1295. https://doi.org/10.1016/j.cjche.2018.09.001

[3] Xiang B, Sun Q, Zhong Q. Current research situation and future prospect of superwetting smart oil/water separation materials. Journal of Materials Chemistry A, 2022, 10(38): 20190-20217. https://doi.org/10.1039/d2ta04469b

[4] Mao J, Deng W, Zhao M. Recent advances in waste-derived sorbents for oil sorption and oil-water separation: progress and future prospects. Separation and Purification Technology, 2026, 402. https://doi.org/10.1016/j.seppur.2026.138659

[5] Zhang W, Liu Y, Tao F. An overview of biomass-based Oil/Water separation materials. Separation and Purification Technology, 2023, 316: 123767. https://doi.org/10.1016/j.seppur.2023.123767

[6] Li B, Qi B, Guo Z. Recent developments in the application of membrane separation technology and its challenges in oil-water separation: A review. Chemosphere, 2023, 327: 138528. https://doi.org/10.1016/j.chemosphere.2023.138528

[7] Pi P, Ren Z, Yang Y. A review of various dimensional superwetting materials for oil–water separation. Nanoscale, 2024, 16(37): 17248-17275. https://doi.org/10.1039/d4nr01473a

[8] Wang B, Feng S, Wang C. Nanostructure-based oil–water separation: mechanism and status. Separations, 2023, 10(11): 569. https://doi.org/10.3390/separations10110569

[9] Fan Q, Lu T, Deng Y. Bio-based materials with special wettability for oil-water separation. Separation and Purification Technology, 2022, 297: 121445. https://doi.org/10.1016/j.seppur.2022.121445

[10] Li J J, Zhou Y N, Luo Z H. Polymeric materials with switchable superwettability for controllable oil/water separation: A comprehensive review. Progress in Polymer Science, 2018, 87: 1-33. https://doi.org/10.1016/j.progpolymsci.2018.06.009

[11] Tian Y, Zhou J, He C. The formation, stabilization and separation of oil–water emulsions: A review. Processes, 2022, 10(4): 738. https://doi.org/10.3390/pr10040738

[12] Sankaranarayanan S, Lakshmi D S, Vivekanandhan S. Biocarbons as emerging and sustainable hydrophobic/oleophilic sorbent materials for oil/water separation. Sustainable Materials and Technologies, 2021, 28: e00268. https://doi.org/10.1016/j.susmat.2021.e00268

[13] Kovaleva L, Zinnatullin R, Musin A. Influence of radio-frequency and microwave electromagnetic treatment on water-in-oil emulsion separation. Colloids and Surfaces A: Physicochemical and Engineering Aspects, 2021, 614: 126081. https://doi.org/10.1016/j.colsurfa.2020.126081

[14] Liu Y, Lin Z, Luo Y. Superhydrophobic MOF based materials and their applications for oil-water separation. Journal of Cleaner Production, 2023, 420: 138347. https://doi.org/10.1016/j.jclepro.2023.138347

[15] Yang W J, Yuen A C Y, Li A. Recent progress in bio-based aerogel absorbents for oil/water separation. Cellulose, 2019, 26(11): 6449-6476. https://doi.org/10.1007/s10570-019-02559-x

[16] Georgios D, John B. Separation of oil/water emulsions in continuous flow using microwave heating. 2013. https://doi.org/10.1021/ef400634n

[17] Usha R Z. Surface-modified polymeric membrane-based separation technology with super-wetting properties for sustainable oily wastewater separation: A cutting-edge review. Separation and Purification Technology, 2026, 380(P1): 135219-135244. https://doi.org/10.1016/j.seppur.2025.135219

[18] Mao T, Xiao R, Liu P. Facile fabrication of durable superhydrophobic fabrics by silicon polyurethane membrane for oil/water separation. Chinese Journal of Chemical Engineering, 2023, 55: 73-83. https://doi.org/10.1016/j.cjche.2022.05.003

[19] Stack L J, Carney P A, Malone H B. Factors influencing the ultrasonic separation of oil-in-water emulsions. Ultrasonics sonochemistry, 2005, 12(3): 153-160. https://doi.org/10.1016/j.ultsonch.2003.10.008

[20] Huang X F, Xiong Y J, Yin W. Demulsification of a new magnetically responsive bacterial demulsifier for water-in-oil emulsions. Energy & Fuels, 2016, 30(6): 5190- 5197. https://doi.org/10.1021/acs.energyfuels.6b00687

[21] Sun N, Dong H, Liu J. Study on the effect of modified magnetic nanoparticles Co_3O_4@ HPAM monomer ratio on viscosity reduction of thick oil emulsification. Chinese Journal of Chemical Engineering, 2026. https://doi.org/10.1016/j.cjche.2025.12.021

[22] Yan S, Jiang P, Zhang X. Advancing oil-water separation: Design and efficiency of amphiphilic hyperbranched demulsifiers. Journal of Colloid and Interface Science, 2025, 677: 583-596. https://doi.org/10.1016/j.jcis.2024.08.101

[23] Ahmadi M, Aliabadian E, Liu B. Comprehensive review of the interfacial behavior of water/oil/surfactant systems using dissipative particle dynamics simulation. Advances in Colloid and Interface Science, 2022, 309: 102774. https://doi.org/10.1016/j.cis.2022.102774

[24] Hassanshahi N, Hu G, Li J. Application of ionic liquids for chemical demulsification: A review. Molecules, 2020, 25(21): 4915. https://doi.org/10.3390/molecules25214915

[25] Bentis A, Boukhriss A, Zahouily M. Functionalization of cotton fabrics by sol-gel method using ionic liquids with high-hydrophobic, excellent water repellent, oil/water separation, and self-cleaning properties. Cellulose, 2023, 30(10): 6719-6740. https://doi.org/10.1007/s10570-023-05276-8

[26] Abdullah M M S, Faqihi N A, Al-Lohedan H A. Application of new oleate-based ionic liquids for effective breaking of water in oil emulsions. Fluid Phase Equilibria, 2023, 568: 113737. https://doi.org/10.1016/j.fluid.2023.113737

[27] Xiaohua L, RA K S, Boelo S. Efficiency and mechanism of demulsification of oil-in-water emulsions using ionic liquids. Energy Fuels, 2016, 30, 7622-7628. https://doi.org/10.1021/acs.energyfuels.6b01415

[28] Sadighian H, Ahmadi E, Mohamadnia Z. Application of imidazolium based ionic liquids grafted on microcrystalline cellulose as demulsifiers for water in crude oil (W/O) emulsions. Carbohydrate Polymers, 2023, 302: 120406. https://doi.org/10.1016/j.carbpol.2022.120406

[29] Atta A M, Al-Lohedan H A, Ezzat A O. Synthesis and application of geminal dicationic ionic liquids and poly (ionic liquids) combined imidazolium and pyridinium cations as demulsifiers for petroleum crude oil saline water emulsions. Journal of Molecular Liquids, 2021, 325: 115264. https://doi.org/10.1016/j.molliq.2020.115264

[30] Sadighian H, Mohamadnia Z, Ahmadi E. Nanomagnetic cyclodextrin decorated with ionic liquid as green and reversible demulsifier for breaking of crude oil emulsions. Carbohydrate Polymers, 2024, 327: 121697. https://doi.org/10.1016/j.carbpol.2023.121697

[31] Liu F, Yang X, Wu X. A dispersive magnetic solid phase microextraction based on ionic liquid-coated and cyclodextrin-functionalized magnetic core dendrimer nanocomposites for the determination of pyrethroids in juice samples. Food chemistry, 2018, 268: 485-491. https://doi.org/10.1016/j.foodchem.2018.06.105

[32] Cheng G, Yuan H, Deng X. Swelling poly (ionic liquid) s for demulsifying oil-in-water emulsion by anion exchange. Polymers for Advanced Technologies, 2022, 33(9): 2798-2806. https://doi.org/10.1002/pat.5733

[33] Ahmadi L, Ahmadi E, Mohamadnia Z. Demulsification of water in crude oil emulsions through magnetic nanocomposites decorated with poly (ionic liquid) s. Journal of Molecular Liquids, 2022, 357: 119162. https://doi.org/10.1016/j.molliq.2022.119162

[34] Xu Z, Zhu Q, Bian J. Preparation of a recyclable demulsifier for the treatment of emulsified oil wastewater by chitosan modification and sodium oleate grafting Fe_3O_4. Journal of Environmental Chemical Engineering, 2021, 9(4): 105663. https://doi.org/10.1016/j.jece.2021.105663

[35] Treder N, Roszkowska A, Oledzka I. Effects of Fe_3O_4 magnetic nanoparticle functionalization with ionic liquids and a double-chained surfactant on the pretreatment of plasma samples during drug extraction. Analytical Chemistry, 2022, 94(48): 16587-16595. https://doi.org/10.1021/acs.analchem.2c01985

[36] Lewandowska K. Effect of an ionic liquid on the physicochemical properties of chitosan/poly (vinyl alcohol) mixtures. International Journal of Biological Macromolecules, 2020, 147: 1156-1163. https://doi.org/10.1016/j.ijbiomac.2019.10.084

[37] Sun N N, Ma Y L, Hu J B. Promotion effect of Fe_3O_4@CPAM with different monomer ratios on microwave demulsification of heavy oil. Acta Petrolei Sinica, 2024, 45(08): 1257-1269. https://doi.org/10.1021/acsomega.3c08238

[38] Wu D, Peng M G, Gu Y. Preparation of magnetic nano-demulsifier and its demulsification performance on heavy oil emulsion. Chemical Industry and Engineering Progress, 2025, 44(01): 436-444. https://doi.org/10.16085/j.issn.1000-6613.2024-0112

[39] Li Y Y, Ma H R, Meng Z C. Preparation and performance of magnetic carbon based nanodemulsifier. Contemporary Chemical Industry, 2025, 54(03): 582-588. https://doi.org/10.13840/j.cnki.cn21-1457/tq.2025.03.030

[40] Cai M M, Du J Z. Preparation of novel bionic magnetic nano-demulsifier and study on its properties. Modern Chemical Industry, 2025, 45(05): 171-174. https://doi.org/10.16606/j.cnki.issn0253-4320.2025.05.028

[41] Qu Q, Li H, Li S. Synthesis and demulsification mechanism of an ionic liquid with four hydrophobic branches and four ionic centers. Chemosphere, 2023, 340: 139802-139812. https://doi.org/10.1016/j.chemosphere.2023.139802

[42] Shen L, Liu S, He J. Synthesis of a low temperature ionic liquid demulsifier and its demulsification mechanism. Fuel, 2023, 338: 127343. https://doi.org/10.1016/j.fuel.2022.127343

[43] Ding Y, Ai G, Du J. Synthesis and demulsification performance of a gemini ionic liquid with dual cationic active centers. Separation and Purification Technology, 2024, 330: 125242. https://doi.org/10.1016/j.seppur.2023.125242

[44] Liu Y G, Yan Y Z, Guo B. Synthesis and demulsification performance of a gemini-type ionic liquid demulsifier. Chemistry & Bioengineering, 2025, 42(06): 62-28. https://doi.org/62-6810.3969/j.issn.1672-5425.2025.06.010